Chinese Chemical Letters 34 (2023) 108197

Contents lists available at ScienceDirect

Chinese Chemical Letters

journal homepage: www.elsevier.com/locate/cclet

Carbon dots with two-photon fluorescence imaging for efficient synergistic trimodal therapy

Yahui Zhang[a,b], Haoyu Xia[a,b], Mengdie Yang[a,b], Hairong Li[a,b], Feishi Shan[a,b], Yilong Chen[a,b], Xue Yue[a,b], Zhouyu Wang[a,b,*], Xiaoqi Yu[a,b,c,*]

[a] Department of Chemistry, School of Science, Xihua University, Chengdu 610039, China
[b] Asymmetric Synthesis and Chiral technology Key Laboratory of Sichuan Province, Chengdu 610039, China
[c] Key Laboratory of Green Chemistry and Technology of Ministry of Education, College of Chemistry, Sichuan University, Chengdu 61064, China

ARTICLE INFO

Article history:
Received 16 December 2022
Revised 5 January 2023
Accepted 6 February 2023
Available online 10 February 2023

Keywords:
Carbon dots (CDs)
Two-photon imaging
Photothermal therapy (PTT)
Type I photodynamic therapy (PDT)
Synergistic trimodal anticancer therapy

ABSTRACT

Applying the fluorescent carbon dots as smart materials in anticancer therapy is of great interest. However, carbon dots for multimodal synergistic anticancer therapy, especially for the triple modality, is rarely reported. Herein, we successfully synthesized OCDs by citric acid and (1*R*,2*S*)-2-amino-1,2-diphenylethan-1-ol, which show aggregation-induced emission property and two-photon fluorescence imaging. Meanwhile, OCDs are ideal photosensitizers for photothermal therapy under 808 nm and Type I photodynamic therapy with white light. Hydroxyl radicals, generated by Type I photodynamic therapy based on OCDs can transform protumoral M2 macrophages into antitumoral M1 macrophages, which exhibited immunotherapy ability. The synergism trimodal of OCDs results in potent anticancer efficacy, showing great potential in cancer therapy.

© 2023 Published by Elsevier B.V. on behalf of Chinese Chemical Society and Institute of Materia Medica, Chinese Academy of Medical Sciences.

Photothermal therapy (PTT) and photodynamic therapy (PDT) have emerged as new modalities for cancer therapy because of their outstanding advantages such as spatiotemporal controllability, minimal invasiveness, high efficiency, and low toxicity [1–6]. For PTT, photothermal agents (PTAs) can convert the input light energy into heat which can induce protein disruption and tumor cells death [7–9]. While in PDT, photosensitizers (PSs) trigger the generation of reactive oxygen species (ROS), which can disrupt cellular membranes, proteins, and nucleic acids, thereby realizing effective treatment [10–14]. According to the mechanism, PDT can be divided into two types: Type I involves an electron or proton transfer generating free radicals such as superoxide anion ($^{\bullet}O_2^-$) and hydroxyl radical ($^{\bullet}OH$), while Type II includes an energy transfer producing singlet oxygen ($^1O_2$) [1,12,15]. It is important to point out that oxygen is necessary for the production of $^1O_2$ in Type II PDT, but the tumor microenvironment is hypoxic [12,16,17]. Therefore, Type I PDT is more advantageous in hypoxic tumor. Additionally, the antitumoral M1 macrophages (M1) exhibiting immunotherapy ability can be transformed from protumral M2 macrophages (M2) in the presence of $^{\bullet}OH$ during Type I PDT process [18,19]. Thus, Type I PDT itself is a combination of photodynamic therapy and immunotherapy.

Considerable efforts have been devoted to endowing carbon dots (CDs) with diverse properties to expand their application fields in anticancer therapy [20–28]. CDs materials are excellent PTAs/PSs candidates for PTT and PDT, due to the unique properties and diverse functions [17,29–32]. However, the single mode phototherapy (PTT or PDT alone) using CDs materials cannot always results in successful therapeutic outcome, as the high temperature and long-time irradiation during the therapy may lead to inflammation and thermal damage to the normal tissues nearby [4,10,11,33]. To overcome the drawbacks of single-mode phototherapy (PTT or PDT) and enhance its efficacy, multiple therapy of CDs had been introduced [34]. Commercially available PSs or anticancer drugs are introduced to form a combination therapy with CDs. Jia *et al.* prepared Ce6-RCDs by covalently coupling red emissive CDs (PTAs) with Ce6 (PSs), which exhibited a much higher cancer therapy efficacy under a low laser power density [35]. Dutta *et al.* prepared CDs with high reactive oxygen species (ROS) generation ability, which were developed to load the doxorubicin (DOX). The CDs-DOX system realized chemotherapy and PDT synergetic therapy [36].

These works achieved synergistic therapy based on CDs by introducing additional therapeutic agents, which increase the cost and complicate the preparation process. Simultaneous synergistic

* Corresponding authors at: Department of Chemistry, School of Science, Xihua University, Chengdu 610039, China.
E-mail addresses: zhouyuwang@mail.xhu.edu.cn (Z. Wang), xqyu@scu.edu.cn (X. Yu).

https://doi.org/10.1016/j.cclet.2023.108197
1001-8417/© 2023 Published by Elsevier B.V. on behalf of Chinese Chemical Society and Institute of Materia Medica, Chinese Academy of Medical Sciences.

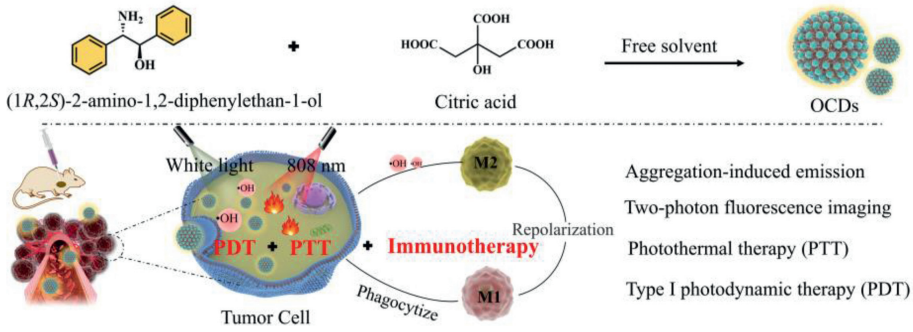

Fig. 1. Synthetic route of OCDs and schematic diagram of synergistic PTT, Type I PDT and immunotherapy processes.

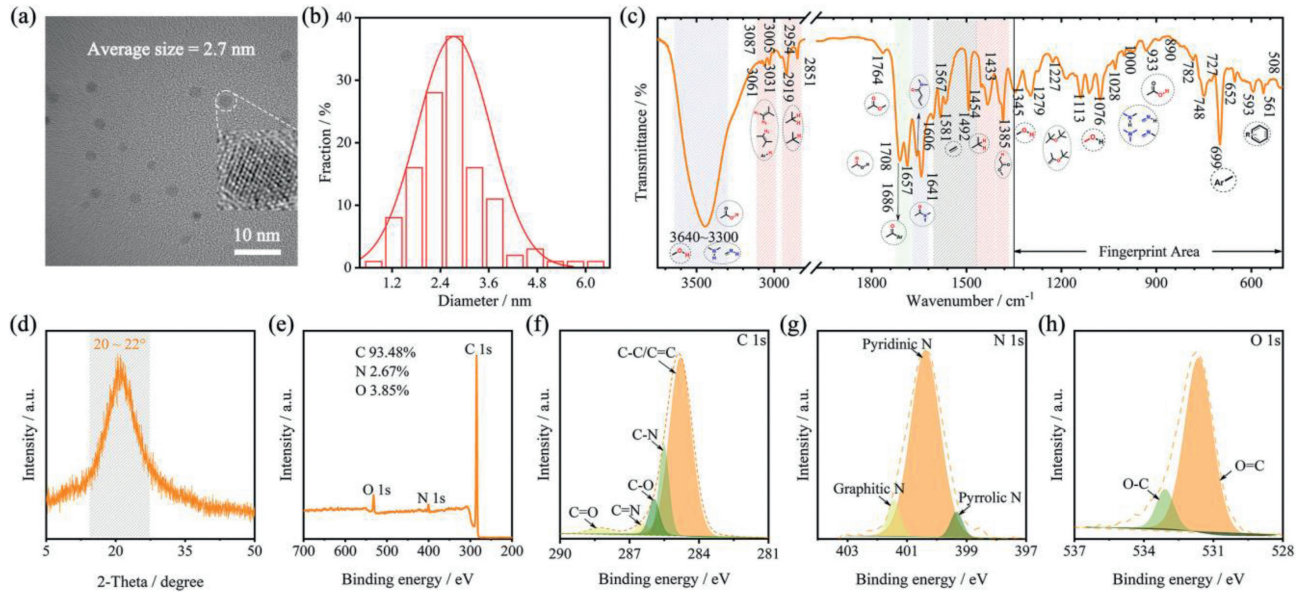

Fig. 2. (a) The transmission electron microscopy (TEM) of OCDs, inset: the high-resolution transmission electron microscopy (HRTEM) of OCDs. (b) The size distribution of OCDs. (c) The Fourier transform infrared spectroscopy (FTIR) of OCDs. (d) The X-ray diffraction (XRD) spectrum of OCDs. (e) The X-ray photoelectron spectroscopy (XPS) of OCDs. The high-resolution (f) C 1s XPS, (g) N 1s XPS, and (h) O 1s spectra of OCDs, respectively.

therapy with individual CDs has gradually attracted attention. Chen *et al.* proposed the carbon dots, which demonstrated an extremely high photothermal conversion efficiency of 77.6% and a high $^1O_2$ quantum yield of 0.37 under a 660 nm light irradiation [37]. However, CDs with superior Type I PDT are still scarce [38].

Herein, we designed and synthesized orange carbon dots (OCDs) by citric acid and (1*R*,2*S*)-2-amino-1,2-diphenylethan-1-ol as shown in Fig. 1 to achieve trimodal therapy. The OCDs have good Type I ROS generation ability and photothermal conversion ability, thus, simultaneously exhibiting three synergistic therapy modalities against cancer, which are PTT, Type I PDT and immunotherapy. Also, aggregation-induced emission (AIE) performance and the two-photon imaging make up for the shortcoming of the short excitation wavelength of OCDs and realize near-infrared (NIR) phototherapy excitation of OCDs. OCDs are very promising candidates for multimodel combination therapy.

In this study, we strategically designed and prepared the OCDs by citric acid and (1*R*,2*S*)-2-amino-1,2-diphenylethan-1-ol as shown in Fig. S1 (Supporting information). The OCDs exhibit a uniform dispersion with an average size of 2.7 nm as confirmed by transmission electron microscopy (TEM) imaging (Fig. 2a), which the size distribution range is 1.0~6.2 nm (Fig. 2b). Meanwhile, the high-resolution TEM (HRTEM) image provides more detailed evidence for the crystalline structure of the OCDs. The lattice spacing is 0.12 nm (Fig. 2a inset) which is different from that of graphene or graphene quantum dots [39,40]. This is attributed to the preparation process of OCDs, which has great influence on the formation of lattice spacing of CDs.

Fourier transform infrared spectroscopy (FT-IR) spectroscopy represents the functional groups of OCDs on the surface, as shown in Fig. 2c. The peaks at 3640~3300, 1345~1279, 933 cm^{-1} are assigned to the stretching vibration of O-H and the peak at 3500~3300, 3087~2851, 1764, 1708~1686 cm^{-1} are assigned to the N-H, C-H, O-C=O and C=O groups, respectively. The stretching vibration peaks of C-N, C=N, C=C and C-C are at 1675~1641, 1028~1000, 1606~1492 and 699~508 cm^{-1}. The FTIR results show that the formation of OCDs conforms to the basic principles of organic synthesis, such as condensation, dehydration, ring-off, addition, cross-linking and carbonization [41].

In addition, The OCDs exhibit relatively obvious diffraction peak near 20°~22° as confirmed by X-ray diffraction (XRD) spectrum, which confirms the existence of the carbon core structure as shown in Fig. 2d [42,43]. And the X-ray photoelectron spectroscopy (XPS) spectrum shows three characteristic peaks (Fig. 2e), corresponding to C 1s (284.80 eV), N 1s (400.38 eV), O 1s (531.64 eV), and the elemental content of C, N, O is 93.48 %, 2.67 %, 3.85 %, respectively. The high-resolution C 1s spectrum (Fig. 2f) exhibitions five peaks at 284.80, 285.51, 285.93, 286.44 and 288.28 eV, which are assigned to C-C/C=C, C-N, C-O), C=N, and C=O, respectively. The N 1s spectrum (Fig. 2g) reveals three different types of

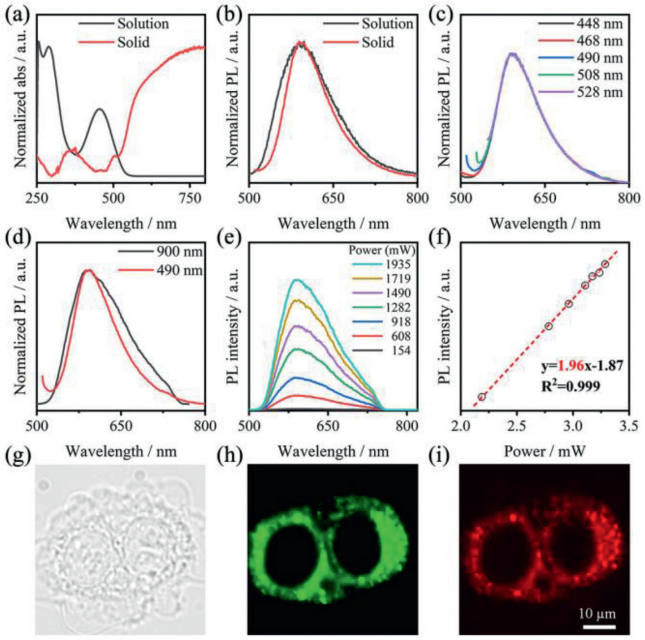

Fig. 3. (a) Absorption and (b) photoluminescence spectra of OCDs. (c) Photoluminescence spectra of OCDs with different excitation wavelength. (d) Emission spectra of OCDs solid excited at 490 nm (red line) and 900 nm (black line). (e) Emission spectra and (f) the logarithmic plots of the emission integral of OCDs solid at different excitation intensities by 900 nm femtosecond pulsed laser light. CLSM images of 4T1 cells incubated with OCDs (10 μg/mL in DMEM): (g) bright field image, (h) λ_{ex} = 490 nm, (i) λ_{ex} = 900 nm.

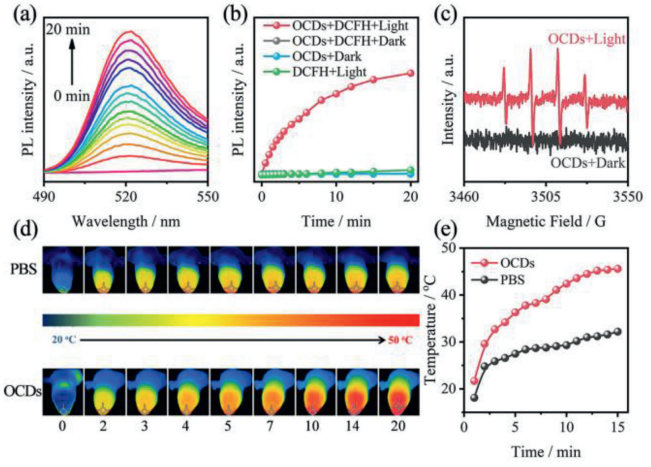

Fig. 4. (a) PL spectra and (b) PL intensity net change at 532 nm for the DCFH indicator with OCDs upon wight light irradiation (10 mW/cm^2), [DCFH] = 1.0×10^{-6} mol/L, [OCD] = 10 μg/mL. (c) Electron paramagnetic resonance spectrometer (EPR) to verify the production of ·OH. (d) The temperature image and (e) the temperature change curve of PBS and OCDs (10 μg/mL) under 808 nm laser irradiation (1 W/cm^2).

N: pyridinic N, pyrrolic N, and graphitic N, respectively. The O 1s shows two peaks at 531.46 and 533.09 eV, assigned to O=C and O-C bonds, respectively (Fig. 2h). The high-resolution spectra of C 1s, N 1s, and O 1s indicates that OCDs have various chemical groups, consistent with the analysis of FTIR.

The absorption and photoluminescence (PL) spectra of OCDs were measured. The prepared OCDs have poor water solubility and are easily soluble in organic solvents. Therefore, DMSO is selected as a good solvent and water is used as a poor solvent to test the optical properties. As shown in Figs. 3a and b, the absorption peak of the solution shows at 448 nm. The emission peak of OCDs in DMSO appears in the orange region at 580 nm and does not change with the excitation wavelength (Fig. 3c). Interesting, with the water content increasing, a new emission peak appears at 480 nm, which achieves its maximum in intensity when the water fraction (f_w) reaches 40%. When the f_w is more than 60%, the emission peak of 480 nm almost disappears and the emission peak of 580 nm plays a dominant role (Fig. S2 in Supporting information). The system displays bright orange emission. When the water content is 99%, the absolute fluorescence quantum yield (ϕ_f) of aggregated OCDs is as high as 10.30, showing typical AIE properties.

Compared with one-photon imaging, two-photon fluorescence imaging excited by NIR laser displays better performance in terms of deeper penetration, lower photo damage, and higher signal-to-noise ratio. We are glad to find that OCDs have the ability of two-photon imaging and it can make up for the shortcoming of the short excitation wavelength of OCDs. The optimal excitation wavelength is determined. As can be seen from the Fig. S3 (Supporting information), OCDs can be excited by 800, 850, 900 and 1000 nm, respectively, among which 900 nm exciting light lead to the strongest florescence emission. The band shape and position are almost the same excited by 490 nm and 900 nm as shown in Fig. 3d. Also, the PL intensity increases with increasing laser power with 900 nm excite. Moreover, relationship between PL intensity and power demonstrate exponential linear relationship (Figs. 3e and f). Subsequently, the two-photon imaging capability of OCDs is validated at the cellular level. As shown in Fig. S4 (Supporting information), the fluorescence image of 4T1 cells indicates that the OCDs might localize at lysosome with a Pearson coefficient of 0.94. Meanwhile, signals of OCDs in 4T1 cell from two-photon imaging irradiated with 900 nm laser display almost identical distribution compared to that of one-photon imaging (490 nm) (Figs. 3g–i). The two-photon imaging capability of OCDs under NIR-light excitation in aqueous solution, makes OCDs potential not only for bioimaging, but also for PTT under 808 nm.

The fluorescent indicator 2′,7′-dichlorodihydrofluorescein (DCFH) was used to evaluate the total ROS generation ability. As shown in Figs. 4a and b, when OCDs with DCFH-DA are irradiated by white light (10 mW/cm^2), the fluorescence intensity at 532 nm increases dramatically, indicating the strong ability of OCDs to generate ROS under white light irradiation. To clarify the types of ROS, the commonly used $^1O_2$ indicator 9,10-anthracenediyl-bis(methylene)-dimalonic acid (ABDA) is used. As shown in Fig. S5 (Supporting information), the absorbance of ABDA hardly changes for OCDs, thereby indicating no $^1O_2$ generation. Meanwhile, electron spin resonance (ESR) spectroscopy is employed. Four-line resonances at a 1:2:2:1 intensity is observed under laser irradiation at 490 nm, which directly confirmed ·OH production (Fig. 4c). These results directly indicates that OCDs belonged to Type I PSs and had an excellent ability to produce Type I ROS (·OH). Photothermal conversion capability is also tested. The temperature of the OCDs solution increases rapidly to 42.4 °C within 10 min under 808 nm laser radiation and reaches 45.6 °C at 20 min as shown in Figs. 4d and e. Temperatures reaching 45 °C can lead to enhanced PDT efficiency. PTT could improve the oxygen supply in the tumor tissue through raising the blood flow rate, thus promoting the PDT effect, which conversely further eliminates the heat-resistant tumor cells in PTT [44,45].

Then we confirmed the combined effect of PDT, PTT and immunotherapy of OCD at the cellular level. Cytotoxicity of different concentrations of OCDs is shown in Fig. S6 (Supporting information). When the concentration of OCD is lower than 10 μg/mL, the cell survival rate is higher than 90%, illustrating non-toxic. In Fig. 5a, 4T1 cells show a strong green fluorescence treated with OCDs under white light, indicating the presence of high levels of

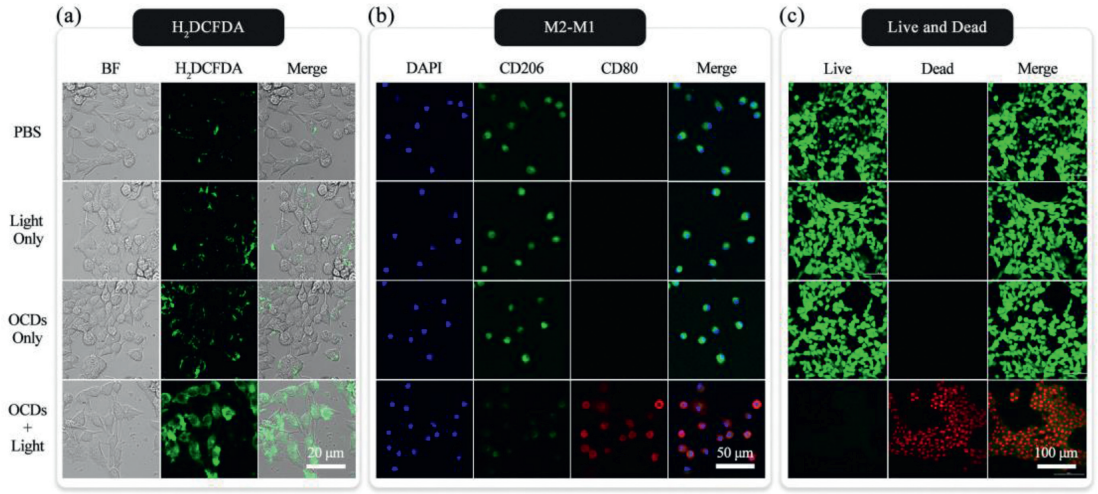

Fig. 5. Fluorescence images by CLSM of 4T1 cells stained with (a) H_2DCFDA. (b) DAPI, CD206 and CD80. (c) Calcein-AM/PI. Light for H_2DCFDA and M2-M1 was white light; Light for Live and Dead was dual light radiation (white light + 808 nm).

ROS. Comparatively, the other three groups of 4T1 cells have almost no green fluorescence or very weak fluorescence. ˙OH generated by OCDs under white light can continuously re-educate M2 to M1 macrophages, which can phagocytose tumor cells exhibiting immunotherapy feasibility. As expected, the cells treated with OCDs under white light significantly increase the expression of M1-related costimulatory molecules CD86 (red emission in Fig. 5b), while decreasing the expression of CD206, a typical marker for the M2 phenotype (green emission in Fig. 5b), suggesting the successful transformation of M2 to M1. Finally, we combine PDT, PTT and immunotherapy to achieve multimodal treatment of cancer cells. As shown in Fig. 5c, 4T1 cells co-incubated with OCDs are almost apoptotic under white light (Type I PDT) and 808 nm laser (PTT) radiation. Compared to the group PBS, group Light Only and OCDs Only, OCDs with dual light radiation display the highest red fluorescence and negligible green fluorescence, confirming that therapeutic synergism is the most effective in killing cancer cells.

OCDs showed good effect *in vitro*, and then we studied PTT/PDT and immunotherapy synergistic therapy of OCDs in tumor bearing mice. The mice were randomly divided into four groups ($n = 5$) when the volume of subcutaneously inoculated 4T1 tumor reached 40 mm^3. The focus of this work was therapeutic effect of synergistic trimodal therapy. Intratumoral injection was used to evaluate the effectiveness of treatment [45,46]. The mice were treated with intratumoral injection of PBS (group PBS, group Light Only) or OCDs (group OCDs Only, group OCDs+Light), followed with or without irradiation as shown in Fig. 6a. As shown in Fig. 6b (the corresponding tumor photographs) and 6c (the tumor growth curves), the tumor volume in the group PBS, group Light Only and group OCDs Only obviously increased.

However, after white light (0.2 W/cm^2, 2 min) and 808 nm irradiation (1 W/cm^2, 10 min), the group OCDs+Light exhibited significant tumor growth inhibition, and tumor is controlled and somewhat or even completely disappeared. Importantly, their body weights were also recorded every two days and no significant change in all four groups was observed (Fig. 6d), demonstrating the good biosafety of our PDT/PTT immunotherapy approach. These results were further confirmed by hematoxylin and eosin (H&E) staining (Fig. S7 in Supporting information) and complete blood panel and serum biochemistry test (Fig. S8 in Supporting information) after the synergistic therapy of OCDs. Then we observed that the proportion of M1 cells in the group OCDs+Light was almost 4.9 times than that of group PBS from dissected and analyzed of the tumors, confirming the participation of immunotherapy in the treatment *in vivo* (Fig. 6e). The above results indicate that the synergistic therapy of OCDs is effective and biofriendly.

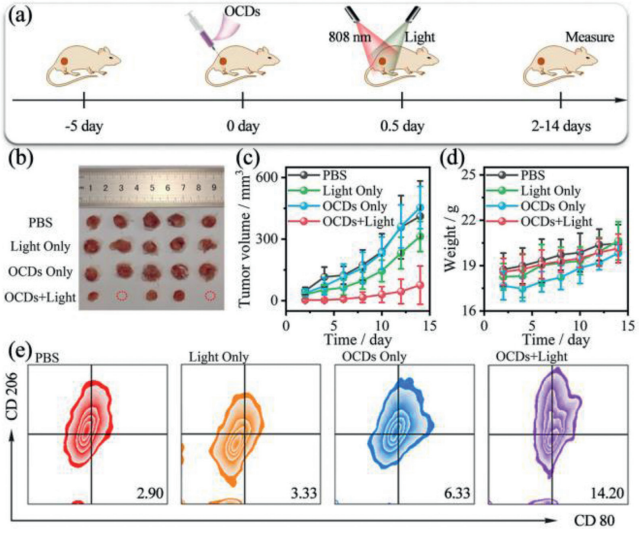

Fig. 6. (a) Treatment schedule. (b) Representative tumor images from mice on the 14th day after treatment. (c) Tumor growth curves for all treated groups. (d) Weights of the tumors collected on day 14 of treatment. (e) Ratios of the M1 phenotype in tumor tissues after treatment with OCDs. Light: white light (0.2 W/cm^2, 2 min) and 808 nm irradiation (1 W/cm^2, 10 min).

In this study, OCDs is obtained by one-step synthesis using citric acid and (1*R*,2*S*)-2-amino-1,2-diphenylethan-1-ol as substrates. The OCDs demonstrate excellent optical properties, typical AIE property and two-photon fluorescence imaging. Moreover, OCDs exhibited excellent ability to generate type I ROS (˙OH) with white light and good photothermal conversion ability under 808 nm irradiation. Type I PDT generated ˙OH can trigger the conversion of M2 cells to M1 cells, leading to immunotherapy. The AIE, two-photon imaging, PDT and PTT capabilities enable OCDs to be used in multimodal combination therapy of tumors. OCDs agent under light irradiation, effectively inhibited tumor growth and prolonged the life of in tumor-bearing mice, thus, demonstrates safe multimodal therapeutic results. Longer emission wavelength and targeting to tumors will become the focus of our future work. To explore the multi-mode synergistic therapy of CDs by intravenous injection.

CDs are biocompatible and available to the *in vivo* system and are expected for clinical treatment.

Declaration of competing interest

The authors declare that they have no known competing financial interests or personal relationships that could have appeared to influence the work reported in this paper.

Acknowledgments

This work was financially supported by the National Natural Science Foundation of China (Nos. 21905021, U21A20308), Sichuan Science and Technology Support Program (Nos. 2022NSFSC1269, 2023NSF1977, 2023NSFSC0637, 2022ZYD0048, 2021ZDYF3218, 2021YFG0291, 2021YFH0132), and Sichuan Students' Platform for innovation and entrepreneurship training program (No. 202210623013).

Supplementary materials

Supplementary material associated with this article can be found, in the online version, at doi:10.1016/j.cclet.2023.108197.

References

[1] X.S. Li, J.F. Lovell, J. Yoon, X.Y. Chen, Nat. Rev. Clin. Oncol. 17 (2020) 657–674.
[2] R. Lima-Sousa, B.L. Melo, C.G. Alves, et al., Adv. Funct. Mater. 31 (2021) 2010777.
[3] H. Jeong, W. Park, D.H. Kim, K. Na, Adv. Drug Deliv. Rev. 177 (2021) 113954.
[4] C. Du, X.J. Wu, M. He, et al., J. Mater. Chem. B 9 (2021) 1478–1490.
[5] Y.J. Hou, X.X. Yang, R.Q. Liu, et al., Int. J. Nanomed. 15 (2020) 6827–6838.
[6] X.Y. Deng, Z.W. Shao, Y.L. Zhao, Adv. Sci. 8 (2021) 2002504.
[7] D.F. Zhi, T. Yang, J. O'Hagan, S.B. Zhang, R.F. Donnelly, J. Control. Release 325 (2020) 52–71.
[8] C. Xu, K.Y. Pu, Chem. Soc. Rev. 50 (2021) 1111–1137.
[9] D. An, J.Y. Fu, B. Zhang, et al., Adv. Funct. Mater. 31 (2021) 2101625.
[10] J.Y. Li, R.Z. Liu, Q. Zhao, et al., Carbon 174 (2021) 90–97.
[11] F.Y. Jin, D. Liu, X.L. Xu, J.S. Ji, Y.Z. Du, Int. J. Nanomed. 16 (2021) 4693–4712.
[12] L. Huang, S.J. Zhao, J.S. Wu, et al., Coord. Chem. Rev. 438 (2021) 213888.
[13] S.Z. Yi, S.M. Deng, X.L. Guo, et al., Carbon 182 (2021) 155–166.
[14] S. Chen, T.T. Sun, M. Zheng, Z.G. Xie, Adv. Funct. Mater. 30 (2020) 2004680.
[15] A. Escudero, C. Carrillo-Carrion, M.C. Castillejos, et al., Mater. Chem. Front. 5 (2021) 3788–3812.
[16] N. Kwon, H. Kim, X.S. Li, J. Yoon, Chem. Sci. 12 (2021) 7248–7268.
[17] B.L. Li, S.J. Zhao, L. Huang, et al., Chem. Eng. J. 408 (2021) 127245.
[18] Q. Wan, R.Y. Zhang, Z.Y. Zhuang, et al., Adv. Funct. Mater. 30 (2020) 2002057.
[19] G. Yang, J.S. Ni, Y.X. Li, et al., Angew. Chem. Int. Ed. 60 (2021) 5386–5393.
[20] C. He, P. Xu, X.H. Zhang, W.J. Long, Carbon 186 (2022) 91–127.
[21] K. Muthamma, D. Sunil, P. Shetty, Appl. Mater. Today 23 (2021) 101050.
[22] D. Qu, Z.C. Sun, Mater. Chem. Front. 4 (2020) 400–420.
[23] T.C. Wareing, P. Gentile, A.N. Phan, ACS Nano 15 (2021) 15471–15501.
[24] B.Y. Wang, H.Q. Song, X.L. Qu, et al., Coord. Chem. Rev. 442 (2021) 204010.
[25] J.J. Liu, R. Li, B. Yang, ACS Central Sci. 6 (2020) 2179–2195.
[26] Y.Q. Wang, X.C. Li, S.J. Zhao, et al., Coord. Chem. Rev. 470 (2022) 204703.
[27] K. Yang, S.J. Zhao, B.L. Li, et al., Coord. Chem. Rev. 454 (2022) 214330.
[28] X.C. Li, X.J. Xing, S.J. Zhao, et al., Chin. Chem. Lett. 33 (2022) 1632–1636.
[29] Y.L. Bai, J.J. Zhao, S.L. Wang, et al., ACS Appl. Mater. Interfaces 13 (2021) 35365–35375.
[30] Y.J. Chung, J. Kim, C.B. Park, ACS Nano 14 (2020) 6470–6497.
[31] B. Chen, M.L. Liu, C.Z. Huang, Trac-Trends Anal. Chem. 134 (2021) 116116.
[32] D. Li, E.V. Ushakova, A.L. Rogach, et al., Small 17 (2021) 2102325.
[33] N. Fernandes, C.F. Rodrigues, A.F. Moreira, I.J. Correia, Biomater. Sci. 8 (2020) 2990–3020.
[34] X.D. Wang, Y.Z. Lin, X. Li, et al., J. Colloid Interface Sci. 507 (2017) 410–420.
[35] Q.Y. Jia, J.C. Ge, W.M. Liu, et al., Nanoscale 8 (2016) 13067–13077.
[36] S.D. Dutta, H.X. Jin, J. Kim, et al., Biomater. Sci. 10 (2022) 1680–1696.
[37] T.X. Chen, T.T. Yao, H. Peng, et al., Adv. Funct. Mater. 31 (2021) 2106079.
[38] Y.A. Tian, Y.X. Huang, X.Y. Huang, Z. Su, F. Wang, New J. Chem. 45 (2021) 14626–14632.
[39] F.S. Shan, L.J. Fu, X.Y. Chen, et al., Chin. Chem. Lett. 33 (2022) 2942–2948.
[40] M.L. Zhang, W.R. Zhang, X. Fan, et al., Nano Lett. 22 (2022) 7203–7211.
[41] F.S. Shan, H.Y. Xia, X.Y. Xie, et al., Microchem. J. 167 (2021) 106273.
[42] H.J. Li, S.C. Han, B.W. Lyu, et al., Chin. Chem. Lett. 32 (2021) 2887–2892.
[43] X.K. Chen, X.D. Zhang, F.G. Wu, Chin. Chem. Lett. 32 (2021) 3048–3052.
[44] B. Li, G.Y. Hao, B. Sun, Z. Gu, Z.P. Xu, Adv. Funct. Mater. 30 (2020) 1909745.
[45] Z.J. Zhang, W.H. Xu, M.M. Kang, et al., Adv. Mater. 32 (2020) 2003210.
[46] T.F. Zhang, J.Y. Zhang, F.B. Wang, et al., Adv. Funct. Mater. 32 (2022) 2110526.